Energy Equip. Sys. / Vol. 8/No. 4/Dec. 2020/ 401-425

ENERGY EQUIPSYS

Energy Equipment and Systems

http://energyequipsys.ut.ac.ir
www.energyequipsys.com

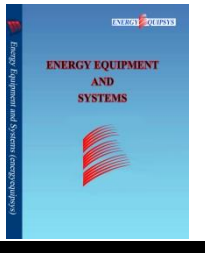

Modeling and optimization of energy consumption and performance characteristics of a solar assisted fluidized bed dryer

Authors

Saeed Mehran[a]
Mohammad Nikian[a*]
Mehrangiz Ghazi[a]
Hemad Zareiforoush[b]
Iraj Bagheri[b]

[a] Department of Mechanical Engineering, Takestan Branch, Islamic Azad University, Takestan, Iran

[b] Department of Mechanization Engineering, Faculty of Agricultural Sciences, University of Guilan, P.O.Box 41635-1314, Rasht, Iran

Article history:

Received : 2 January 2020
Accepted : 17 May 2020

ABSTRACT

The major problem regarding conventional rice mills is the use of fixed-bed drying systems, which is accompanied by high energy consumption. In this study, a novel solar-assisted fluidized-bed system for drying paddy grains was used. The system included a solar water heater, an infrared lamp powered by photovoltaic panels, along with a gas water heater, which were used together to provide the required thermal energy. The working factors were drying air temperature (35, 45, and 55 °C), drying air velocity (7, 8, and 9 m/s), and the angle of the desiccant wheel regeneration gate (0, 45, and 90 degrees). The performance characteristics of the drying system were measured in terms of drying rate, total energy consumption, solar fraction and energy efficiency. Several mathematical models were also applied to fit the moisture ratio curves. In order to analyze the results and obtain the optimized working conditions of the drying system, Response Surface Methodology (RSM) based on the Box–Behnken technique was used. In all of the evaluated conditions, the model entitled "Approximation of diffusion" had the best results for fitting the moisture ratio curves with a correlation coefficient value of at least 0.9729. The selected optimum point included drying air velocity of 7 m/s, drying air temperature of 52.77 ºC and regeneration gate angle of 0. Under the mentioned working conditions, the drying time of 75.99 min, the total energy consumption of 0.297 kWh, solar energy fraction of 0.540 and energy efficiency of 47.67% could be obtained with a desirability value of 0.970.

Keywords: Energy, Solar, Modeling, Optimization, Dryer.

1. Introduction

The strong dependence of industrial societies on energy resources, especially fossil fuels, and their excessive utilization and application drains enormous resources that have been formed in the lower layers of the earth over the centuries. Given that the underground energy sources are being used at an increasing rate, a small amount of the sources will remain in the near future. So, the current generation must pay attention to provide those energy sources with long life and power and develop knowledge to enhance the exploitation of new energy resources. New renewable energy sources are very diverse. Wind energy, geothermal energy, bioenergy, wave energy, tidal energy and hydropower energy are some of these new energy sources. Of course, all these new energy sources have existed since ancient times, but the growth of science and technology has lately enabled humans to

* Corresponding author: Mohammad Nikian
[a] Department of Mechanical Engineering, Takestan Branch, Islamic Azad University, Takestan, Iran
Email: m.nikiyan@tiau.ac.ir

exploit and control these energies. With the growing trend of industrialization in most developing countries and the increasing population globally, the need for various types of renewable energy is being increased. Reducing CO_2 emission by using renewable energy instead of fossil fuels is one of the main challenges for sustainable development [1].

As a growing country with rich and extensive energy resources, Iran is one example of the growth pattern with an emphasis on the use of natural reserves. In Iran, about 98% of the total energy consumption is related to hydrocarbon products, and approximately 70% of the country's foreign exchange earnings come from oil sales. The agricultural sector is one of the major energy-consuming sectors in this country. Energy is an important input in the agricultural sector. The study of energy consumption in the agricultural sector shows that in recent years, with the increase in production and value-added, the consumption of various energy carriers, including petroleum products and electricity, has been increased. The production in the agricultural sector depends largely on fossil fuels, so any disorder in fossil fuel production affects the level of agricultural production. The statistics show that the total energy consumption in the agricultural sector of Iran increased from 33.1 to 43.4 million barrels of oil equivalent from 1991 to 2009 [2].

One of the major agricultural crops in Asian countries is rice, which is widely consumed in most people's meals. The rice plant's final product includes paddy grains transported to rice mills after being harvested from rice fields. The moisture content of paddy grains at the beginning of processing operation is usually more than 20% (w.b.), and it should be reduced to around 10% (w.b.) [3, 4]. For this purpose, drying systems are used prior to rice de-husking, whitening, polishing and sizing machines in rice mills. Approximately in all of the rice processing factories of Iran, fixed-bed type drying systems are used, which consume fossil fuels, chiefly gas. The major problem regarding conventional rice mills is the use of fixed-bed drying systems whose application is accompanied by non-uniform heat transfer in the drying bed. Another problem associated with the use of fixed-bed drying systems is high energy consumption during the drying process. It has been indicated that more than 80 percent of total energy during the rice milling process is consumed by fixed-bed drying systems [5]. Among the various methods for product drying, the fluidized-bed method is of particular significance. The uniformity of moisture distribution across the bed, high rates of mass and heat transfer between the hot air and particles, sufficient mix, and facilitated particle transfer are the positive results derived from the use of fluidized-bed drying systems [6-9].

In recent years, several studies have been conducted concerning the evaluation of the drying process of agricultural products using solar drying systems [10-15]. Shirinbakhsh and Amidpour [16] developed a solar-assisted conveyer-belt dryer for biomass drying and performed its economic Optimization under different conditions. Nazgelichi et al. [17] investigated the effect of factors such as fruit size, bed thickness, and airflow velocity on the carrot drying process using a fluidized-bed drying system. Nassiri and Etesami [18] investigated the energy efficiency for three drying methods, namely, continuous bed drying, indirect solar drying, and hybrid solar drying, with applying three drying temperatures of 35, 45, and 55 °C. Results of their study indicated that the total energy efficiency per unit mass of evaporated water in the continuous bed drying method was lower than the two other methods. Ziaforoughi and Esfahani [15] examined the energy consumption in the potato drying process using a photovoltaic-solar collector-assisted intermittent infrared dryer. They reported that, by using their developed solar system, the amount of electric energy consumption and product drying time reduced by 40-69% and 31-52% compared to nonrenewable infrared lightning.

One of the most important things to do with any type of crop drying system is to monitor the crop drying process and optimize the drying system performance to achieve the highest drying rate and lowest energy consumption. The inappropriate

combinations of air temperature and air velocity during the drying process can result in over-drying or improper drying, leading to reduced product quality and reduced shelf life. It is important to find the optimum process conditions to have the best quality properties in such cases. Several research works have been conducted for modeling and Optimization of different paddy drying systems. Jafari et al. [19] studied the mathematical modeling of paddy drying in a semi-industrial continuous band microwave dryer. Nosrati et al. [20] conducted research aiming to model and Optimize paddy drying in a hot air-infrared radiation vibratory bed dryer. Gharnasi Gharavi et al. [21] used a laboratory rotary dryer machine and response surface methodology (RSM) with a central composite design to model and optimize the drying conditions of paddy grains. The independent factors in their research included drying temperature (40 to 80°C), cylinder rotation speed (2 to 10 rpm) and the cylinder fullness (25 to 66%). Pourbagher et al. [22] studied the drying process of paddy in an infrared and warm air fluidized bed dryer. They used the genetic algorithm method to optimize the dryer performance characteristics by considering cracked grains, milling recovery, degree of milling and drying time. Elhami et al. [23] applied an adaptive neuro-fuzzy inference system (ANFIS) and linear regression models to analyze the energy and economics of lentil and chickpea production. There are several studies in which the Optimization of the drying process of paddy grains have been conducted [24-29]. A comprehensive review was also found in the literature in this field [30].

In the current research, the performance analysis and Optimization of a solar-assisted fluidized-bed paddy dryer are carried out. The proposed dryer benefits from a solar water heater, infrared lamps and gas water heater to supply the required thermal energy for paddy grains drying. The main originalities of the present work are listed as follows:

- The combination of a solar water heater, solar-powered infrared lamps and gas water heater has not been used for grains drying so far.
- In the proposed drying system, a desiccant wheel mechanism is used to help the dehydration process of paddy grains throughout the drying process.
- An adjustable gate is also used in a special regeneration cycle in the drying system to enhance the dehydration ability of the desiccant wheel.
- Solar-powered infrared lamps are used adjacent to the glass wall of the fluidizing chamber to help the dehydration process.
- The mathematical modeling of the dehydration rate indicators is conducted for the proposed hybrid solar dryer.
- The performance characteristics of the developed drying system are evaluated using analytical modeling techniques, which can help the researchers to understand the dynamics of the dryer.
- In order to find the best drying treatment, the working conditions of the drying system are optimized using Response Surface Methodology (RSM).

2. Materials and methods

2.1. Sample preparation

Experiments were conducted from July 2018 to September 2018. Hashemi variety of paddy grains was provided from the research rice field of the University of Guilan, Rasht, Iran. The initial moisture content of the samples was determined utilizing a hot air oven at the temperature of 103 °C for 24 h using [31]

$$MC_{db} = \frac{M_w - M_d}{M_d} \times 100, \quad (1)$$

where M_w is the initial mass of sample (g), M_d is the ultimate mass of sample (g), and MC_{db} is the product moisture based on the dry mass (d.b%).

2.2. System and experiment design

A solar-assisted fluidized-bed drying system was used for drying paddy grains. The system chiefly consisted of a solar water heater and infrared lamp powered by photovoltaic panels (as the primary and main heating sources, both of which worked by

solar energy) along with a gas water heater (as the secondary heating source). The overall setup, together with the schematic of the system working procedure, is illustrated in Fig. 1. First, the environmental air is sucked into the drying system using a centrifugal fan (situation 1). Then the air goes through a desiccant wheel mechanism to reduce its moisture content. In situation 2, a heat exchanger of tube-fin-type, supplied by a thermosiphon-type solar water heater, is used to increase the air temperature. In situation 3, the major part of the heated air is directed into the fluidizing chamber to dry the product. In situation 4, the minor part of the airflow, whose amount can be adjusted by a gate, passes through a copper-plate type heat exchanger. The hot air regenerates the desiccant wheel in situation 5. The air leaving the drying chamber still has thermal energy. Therefore, it is added to the inlet air in situation 1. The system was equipped with a solar-powered 250 W infrared lamp located adjacent to the fluidizing chamber's glass wall.

In the initial stage of drying, the required thermal energy was provided by the solar water heater and solar-powered infrared lamp. During conditions in which the solar water heater could not supply the required thermal energy for the product drying, using an electric valve, a gas water heater received the water flow and provided the required heat for the drying process. The temperature and relative humidity of the drying air were measured using a temperature/ relative humidity sensor (AM2301/DHT21, Model China). The sensors were connected to a computer using an Arduino interface board (Arduino Uno SMD, China). The velocity of the inlet drying air was measured by a digital anemometer (Lutron Model YK, 80 Am, Taiwan).

At each test, 500 g of paddy grains were put in the drying chamber. The experiments were carried out to reduce the moisture content of paddy grains from the initial value of about 25±1% (d.b.) to the final value of 10±1% (d.b.). Before starting each test, the dryer was run according to the defined working conditions to reach the thermal steady state. The working factors included drying air temperature (at three levels of 35, 45, and 55 °C), drying air velocity (at three levels of 7, 8, and 9 m/s), and the angle of desiccant wheel regeneration gate (at three levels of 0, 45, and 90 degrees). The angle of the regeneration gate was considered an affecting factor on the performance of the drying system. According to Fig. 1b, it was assumed that such a factor could influence the regeneration rate of the desiccant wheel mechanism, which affected the drying time and energy consumption of the dryer. The performance characteristics of the drying system were measured in terms of drying time, total energy consumption, solar energy fraction and energy efficiency, which will be defined in the following.

a)

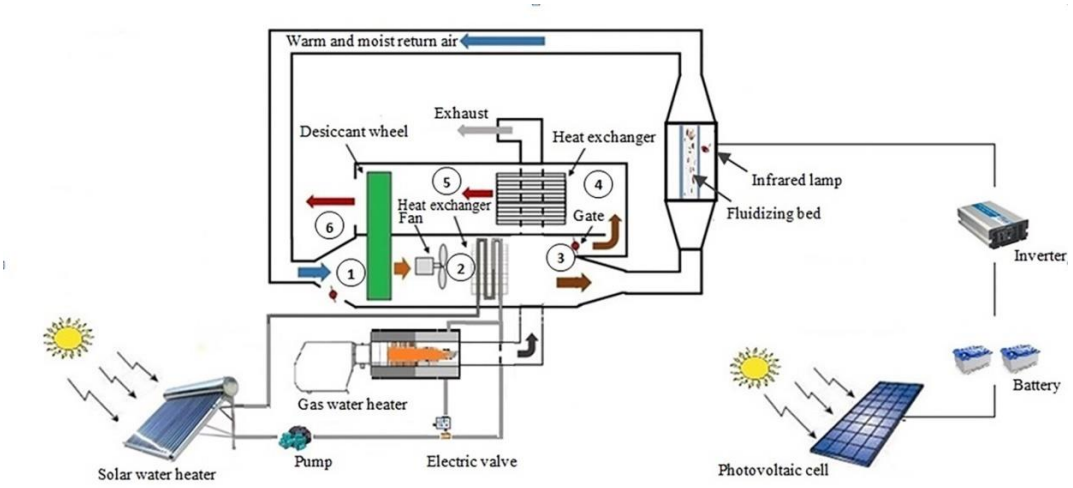

b)

Fig. 1. a) Experimental setup and b) Schematic of solar-assisted dryer working procedure.

2.3. Calculations and measurements

2.3.1.Drying rate

The drying rate was calculated using[32]

$$DR = \frac{(M_{t+dt} - M_t)}{d_t}, \quad (2)$$

where M_t is instantaneous moisture content, M_{t+dt} is moisture content at the time (t+dt) (kg water/kg dry matter), and t is drying time (min).

2.3.2.Moisture ratio

The moisture ratio, the indicator of paddy grains dehydration rate during the drying process, was calculated as follows [33]:

$$MR = \frac{M_t - M_e}{M_0 - M_e} \quad (3)$$

In the above equation, M_t, M_0, and M_e represent instantaneous moisture content, initial moisture content, and equilibrium moisture content of the product (% d.b.), respectively. Since the value of M_e is usually less than those of M_t and M_0, M_e is usually omitted from the above-mentioned equation [34]. Therefore, Eq. (3) is simplified as

$$MR = \frac{M_t}{M_0}. \quad (4)$$

In order to determine the calculate the instantaneous moisture content (M_t), the equation

$$M_t = \left(\frac{W_0(M_0 - 1) + W}{W}\right) \quad (5)$$

was used [35], where W_0 and W are the initial mass of the fresh sample (g) and instantaneous mass of the drying product at any given time (g), respectively. The instantaneous mass of the product was measured using a digital scale with an accuracy of 0.001 (A&D Model GX-1000, Japan).

2.3.3. Total energy consumption

The total energy consumption of the drying system (E_t) was calculated using

$$E_{ns} = E_{wh} + E_{cf} + E_{dw}, \quad (6)$$

where E_{wh}, E_{cf} and E_{dw} were calculated as described in the following sections..

2.3.3.1. Energy consumption of the gas water heater

The energy consumption of the gas water heater was calculated using [36]

$$(E_p)_{wh} = V_g \times E_{eq}. \quad (7)$$

In the equation above, V_g is the volume of natural gas consumed by the water heater in each experiment (m^3), and E_{eq} is the energy

equivalent of natural gas (kWh/m^3). The energy equivalent of natural gas in Iran is 8600 kcal equal to 9.99 kWh/m^3 [37].

2.3.3.1. Energy consumption of the centrifugal fan

The energy consumed by the centrifugal fan of the drying system was measured using[35]

$$(E_p)_{cf} = \Delta P_t \times Q_a \times t\,, \quad (8)$$

where Q_a is the fan volumetric airflow (m^3/s), t is drying time (s), and ΔP is total pressure drop (kPa).

2.3.3.2. Energy consumption of desiccant wheel

The energy consumption of the desiccant wheel was calculated as

$$(E_p)_{dw} = V_w I_w t_w\,, \quad (9)$$

where V_w, I_w, and t are the voltage (V), electrical current (A), and working time of the desiccant wheel drive motor, respectively. It should be noted that during the solar-assisted test conditions, the electrical energy for the drive motor of the desiccant wheel was provided by the photovoltaic system.

2.3.4. Solar energy fraction

The solar energy fraction is a dimensionless ratio referring to the part of the total energy consumption of the drying system provided by the sun. This index was calculated using[38]

$$SF = \frac{E_s}{E_s + E_{ns}}, \quad (10)$$

where E_s is the provided solar energy for supplying the solar water heater and drive motor of the desiccant wheel mechanism (kWh), and E_t is the total energy consumed by the drying system (kWh).

2.3.5. Energy efficiency

Based on the first law of thermodynamics and using the energy balance equation, energy efficiency was calculated using[35]

$$\eta_e = \frac{E_w}{E_t}\,, \quad (11)$$

where E_w is the energy required for moisture evaporation (kJ), and it was calculated using

$$E_w = h_{fg}.m_w\,, \quad (12)$$

where h_{fg} is the latent heat of vaporization (kJ/kg). The two following equations were used to calculate h_{fg} (J/kg) in terms of absolute temperature:

$$h_{fg} = 2.503 \times 10^6 - 2.386 \times 10^3 (T_{abs} - 273.16) \quad 273.16 \leq T_{abs}(k) \leq 338.72, \quad (13)$$

$$h_{fg} = (7.33 \times 10^{12} - 1.60 \times 10^7 {T_{abs}}^2)^{0.5} \quad 338.72 \leq T_{abs}(k) \leq 533.16. \quad (14)$$

2.4. Mathematical modeling of MR curves

Some mathematical models have been used in the literature for describing the drying process of food and crops. Modeling helps design engineers make sound decisions to select proper operational conditions, equipment dimensions, and drying chamber based on the existing conditions. The mathematically modeling principle fits a suitable mathematical equation to the drying data to achieve the best condition in which the system dynamics can be explained. These models are determined as functions of moisture ratio. They are generally derived by simplifying Fick's second law's general series solutions and considering a direct relationship between the average water content and drying time [39]. In the current study, 10 general mathematical models were applied to fit the moisture ratio curves (Table 1). The related references to the equations have been cited by Minaei et al. [40].

Three different criteria, including correlation coefficient (R^2); chi-squared, (χ^2), and root mean square error (RMSE), were used to investigate the fitness of mathematical models. These parameters were calculated using the following Eqs. (15), (16) and (17) [41]

$$R^2 = \frac{\sum_{i=1}^{N}(MR_i - MR_{pre,i})\sum_{i=1}^{N}(MR_i - MR_{\exp,i})}{\sqrt{\left[\sum_{i=1}^{N}(MR_i - MR_{pre,i})^2\right]\cdot\left[\sum_{i=1}^{N}(MR_i - MR_{\exp,i})^2\right]}} \quad (15)$$

Table 1- Mathematical models reported in the literature for describing the drying process of agricultural products

Model name	Model equation	Reference
Wang and Singh	$MR = 1 + at + bt^2$	(Wang and Singh, 1978)
Henderson and Pabis	$MR = a \cdot \exp(-kt)$	(Chhinnan, 1984)
Logarithmic	$MR = a \cdot \exp(-kt) + c$	(Yaldiz et al., 2001)
Approximation of diffusion	$MR = a \cdot \exp(-kt) + (1-a) \cdot \exp(-kbt)$	(Kassem, 1998)
Page	$MR = \exp(-kt^n)$	(Page, 1949)
Two-term	$MR = a \cdot \exp(-kt) + b \cdot (-kt)$	(Henderson, 1974)
Newton	$MR = \exp(-kt)$	(Jayas et al., 1991)
Simplified Fick's diffusion	$MR = a\exp(-c(t/L^2))$	(Kassem, 1998)
Modified Page	$MR = a\exp(-c(t/L^2)^n)$	(Kassem, 1998)
Midilli and Kucuk	$MR = a \cdot \exp(-kt)^n) + bt$	(Midilli et al., 2002)

$$RMSE = \left[\frac{1}{N}\sum_{i=1}^{N}(MR_{pre,i} - MR_{\exp,i})^2\right]^{\frac{1}{2}} \quad (16)$$

and

$$\chi^2 = \frac{\sum_{i=1}^{N}(MR_{\exp,i} - MR_{pre,i})^2}{N-n}; \quad (17)$$

where $MR_{exp,i}$ and $MR_{pre,i}$ are the experimental and predicted moisture ratio, respectively. N is the number of observations, and n is the number of drying constants.

The most appropriate model for describing moisture ratio during drying process of paddy grains was characterized by the highest R^2 and the lowest χ^2 and RMSE values [41-43]. The multivariate regression analysis of MR data was performed in MATLAB software.

2.5. Modeling and Optimization

Response Surface Methodology (RSM) is one of the most common and effective methods to draw a response surface in the desired range, Optimization of the response, or to select the process conditions for achieving target specifications [44]. In this study, in order to analyze the results and obtain the optimized drying condition, RSM based on Box–Behnken was used. The experimental data were analyzed using Design Expert Software (version 10.0.3). The dependent variables in this study were drying time, energy consumption, and solar fraction in the product's drying process. For each independent variable, namely drying air temperature, drying air velocity, and status of the desiccant regeneration gate, three levels of code (-1, 0 and +1) were considered. Table 2 shows the levels of selected independent variables. The response variables for describing the optimum relationship between responses and independent variables were fitted to a second-order polynomial model based on the following Eq. [6]:

$$Y_i = \beta_o + \sum \beta_j X_i + \sum \beta_{ij} X_i X_j + \sum \beta_{jj} X_i^2 + \varepsilon, \quad (18)$$

where β_o, β_i, β_{ij} and β_{ij} are constants, x_i and x_j are independent variables in the process, and ε is random error.

Table 2- Levels and coded values of independent variables

Independent variable	Coded values		
	-1	0	1
A: Drying air temperature (°C)	35	45	55
B: Drying air velocity (m/s)	7	8	9
C: Angle of desiccant regeneration gate (degree)	0	45	90

3. Results and discussion

In the following subsections, the analyses of drying rate, mathematical modeling of DR and analytical modeling of the performance characteristics of the drying system are given. Finally, the optimum condition of the proposed drying system is determined using RSM.

3.1. Drying rate

Figure 2 shows the drying trend of paddy grains with respect to the three evaluated factors during the drying process. In each chart, it can be seen that at the initial stage of the drying process, the drying rate increased rapidly to reach its peak value. This was due to increased moisture release from the inside to the product surface. At the second stage, the drying rate was reduced with a high slope. At the final stage, the drying rate varies with low tolerances and reaches its ultimate point in a lengthier time. With the increase of the drying air temperature, the drying rate curves were higher in their related chart, which means that the drying process has higher speeds. Similar results have been reported by researchers concerning the effect of temperature on the slope of the drying rate [45, 46].

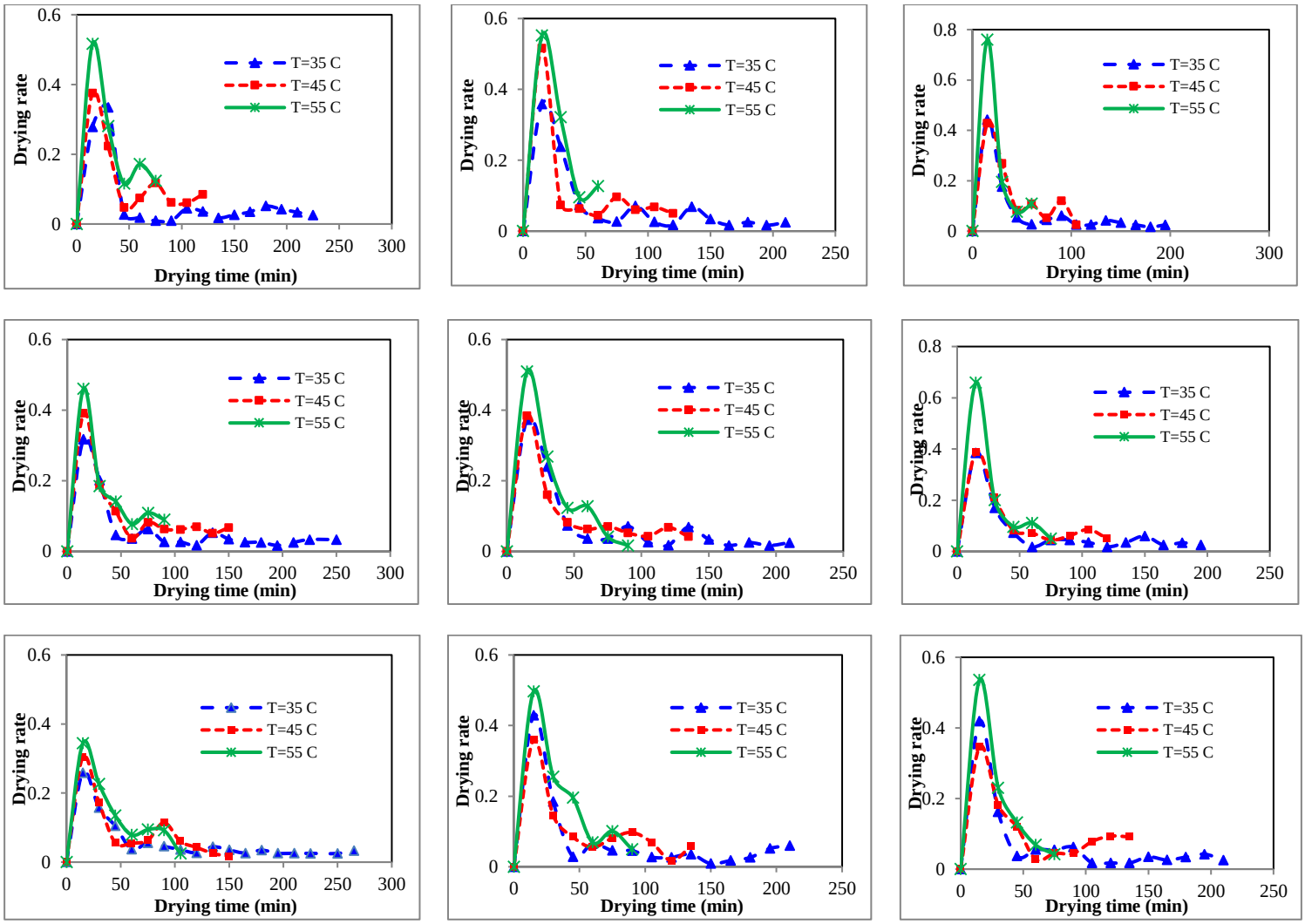

Fig 2. Effect of drying air temperature on drying rate. In each row, the first, second and third charts represent drying air velocities of 7, 8 and 9 m/s, respectively. In each column, the first, second and third charts represent gate angles of 0, 45 and 90 degrees, respectively.

By comparing the charts in each row of Fig. 2, it can be concluded that increasing the drying air velocity caused the drying rate to be increased. Similar conclusions have been drawn by researchers in this field [39, 47, 48]. The charts in each column of Fig. 2 indicate that the drying rate decreased by increasing the desiccant regeneration gate angle. At 90 degree angle of the regeneration gate, the hot air's maximum volume is transferred from the inlet part of the drying chamber to the desiccant wheel. Consequently, the air volume required for the product drying is reduced, which slows down the drying process.

3.2. Mathematical modeling of drying curves

Several mathematical models were evaluated with respect to R^2, RMSE and χ^2 indices. The superior models were selected according to a higher amount of R^2 and lower values of χ^2 and RMSE. The moisture ratio models with their related statistical values at different levels of drying air velocity, drying air temperature and angles of regeneration gate are given in Table 3.

Table 3. Statistical indices of mathematical models applied for moisture ration of paddy grains under different drying conditions

Air temperature (°C)	Gate angle	*0*			*45*			*90*		
	Model name	R^2	$\chi2$	RMSE	R^2	$\chi2$	RMSE	R^2	$\chi2$	RMSE
	Wang and Singh	0.849	0.047	0.059	0.915	0.028	0.045	0.953	0.018	0.034
	Henderson and Pabis	0.811	0.058	0.064	0.866	0.044	0.054	0.914	0.032	0.045
	Logarithmic	0.910	0.028	0.046	0.956	0.014	0.032	0.9776	0.008	0.024
	Approximation of diffusion	**0.973**	**0.008**	**0.025**	**0.998**	**0.001**	**0.007**	**0.999**	**0.000**	**0.004**
	Page	0.956	0.014	0.031	0.993	0.002	0.012	0.997	0.001	0.007
	Two-term	0.959	0.014	0.034	0.998	0.0001	0.008	0.999	0.000	0.004
	Newton	0.544	0.141	0.097	0.620	0.124	0.088	0.759	0.090	0.073
	Simplified Fick's diffusion	0.811	0.058	0.067	0.866	0.044	0.056	0.914	0.032	0.046
	Modified Page equation-II	0.843	0.048	0.063	0.993	0.002	0.013	0.997	0.001	0.008
	Midilli and Kucuk	0.957	0.013	0.033	0.994	0.002	0.013	0.997	0.001	0.008
		Air velocity: 8 (m/s)								
	Wang and Singh	0.914	0.029	0.049	0.916	0.027	0.049	0.877	0.037	0.053
	Henderson and Pabis	0.849	0.051	0.063	0.849	0.052	0.063	0.829	0.051	0.060
	Logarithmic	0.965	0.012	0.031	0.967	0.011	0.031	0.937	0.019	0.038
	Approximation of diffusion	**0.996**	**0.001**	**0.010**	**0.996**	**0.001**	**0.009**	**0.995**	**0.002**	**0.011**
	Page	0.991	0.003	0.015	0.992	0.003	0.014	0.989	0.003	0.015
35	Two-term	0.996	0.001	0.011	0.997	0.001	0.010	0.994	0.002	0.011
	Newton	0.636	0.124	0.094	0.633	0.125	0.094	0.517	0.144	0.098
	Simplified Fick's diffusion	0.849	0.051	0.065	0.849	0.052	0.066	0.829	0.051	0.063
	Modified Page equation-II	0.991	0.003	0.016	0.992	0.003	0.015	0.989	0.003	0.017
	Midilli and Kucuk	0.991	0.003	0.016	0.993	0.002	0.015	0.991	0.003	0.015
		Air velocity: 9 (m/s)								
	Wang and Singh	0.889	0.033	0.055	0.899	0.028	0.051	0.891	0.031	0.051
	Henderson and Pabis	0.818	0.055	0.068	0.848	0.043	0.059	0.827	0.049	0.062
	Logarithmic	0.954	0.014	0.035	0.950	0.014	0.035	0.952	0.014	0.034
	Approximation of diffusion	**0.999**	**0.000**	**0.006**	**0.998**	**0.001**	**0.007**	**0.997**	**0.001**	**0.008**
	Page	0.996	0.001	0.009	0.993	0.002	0.013	0.995	0.001	0.010
	Two-term	0.995	0.000	0.019	0.995	0.000	0.019	0.997	0.001	0.008
	Newton	0.544	0.138	0.103	0.611	0.109	0.092	0.534	0.134	0.098
	Simplified Fick's diffusion	0.818	0.055	0.071	0.848	0.043	0.062	0.827	0.049	0.064
	Modified Page equation-II	0.996	0.001	0.011	0.993	0.002	0.014	0.995	0.001	0.011
	Midilli and Kucuk	0.996	0.001	0.010	0.994	0.002	0.013	0.996	0.001	0.010
45		Air velocity: 7 (m/s)								

Wang and Singh	0.960	0.009	0.040	0.953	0.014	0.041	0.970	0.008	0.032
Henderson and Pabis	0.936	0.016	0.047	0.929	0.021	0.048	0.940	0.016	0.043
Logarithmic	0.978	0.005	0.030	0.975	0.007	0.030	0.981	0.005	0.026
Approximation of diffusion	**0.973**	**0.007**	**0.033**	**0.998**	**0.001**	**0.007**	**0.993**	**0.002**	**0.015**
Page	0.993	0.002	0.015	0.996	0.001	0.012	0.993	0.002	0.015
Two-term	0.996	0.001	0.014	0.998	0.000	0.008	0.993	0.002	0.016
Newton	0.884	0.028	0.059	0.851	0.044	0.066	0.877	0.033	0.058
Simplified Fick's diffusion	0.936	0.016	0.051	0.929	0.021	0.051	0.939	0.016	0.045
Modified Page equation-II	0.993	0.002	0.018	0.996	0.001	0.013	0.993	0.002	0.017
Midilli and Kucuk	0.995	0.001	0.016	0.997	0.001	0.011	0.993	0.002	0.016
	Air velocity: 8 (m/s)								
Wang and Singh	0.899	0.023	0.062	0.951	0.012	0.042	0.965	0.009	0.035
Henderson and Pabis	0.864	0.031	0.067	0.909	0.023	0.000	0.938	0.015	0.044
Logarithmic	0.939	0.014	0.048	0.979	0.005	0.028	0.979	0.005	0.027
Approximation of diffusion	**0.995**	**0.001**	**0.013**	**0.999**	**0.000**	**0.003**	**0.997**	**0.001**	**0.009**
Page	0.986	0.003	0.021	0.998	0.000	0.007	0.996	0.001	0.011
Two-term	0.998	0.000	0.009	0.999	0.000	0.004	0.997	0.001	0.010
Newton	0.7384	0.059	0.086	0.818	0.046	0.071	0.874	0.031	0.059
Simplified Fick's diffusion	0.864	0.031	0.072	0.909	0.023	0.057	0.938	0.015	0.047
Modified Page equation-II	0.961	0.009	0.042	0.998	0.000	0.008	0.996	0.001	0.013
Midilli and Kucuk	0.989	0.000	0.007	0.999	0.000	0.007	0.997	0.001	0.011
Wang and Singh	0.953	0.014	0.041	0.952	0.012	0.044	0.937	0.016	0.049
Henderson and Pabis	0.929	0.021	0.048	0.909	0.022	0.056	0.923	0.020	0.050
Logarithmic	0.975	0.007	0.030	0.982	0.004	0.027	0.961	0.010	0.038
Approximation of diffusion	**0.998**	**0.000**	**0.007**	**0.998**	**0.001**	**0.009**	**0.989**	**0.003**	**0.020**
Page	0.996	0.001	0.012	0.995	0.001	0.012	0.984	0.004	0.023
Two-term	0.998	0.000	0.008	0.998	0.001	0.010	0.989	0.003	0.022
Newton	0.851	0.044	0.066	0.836	0.039	0.070	0.856	0.038	0.065
Simplified Fick's diffusion	0.929	0.021	0.051	0.909	0.022	0.060	0.923	0.020	0.054
Modified Page equation-II	0.995	0.001	0.014	0.995	0.001	0.015	0.928	0.019	0.056
Midilli and Kucuk	0.997	0.001	0.011	0.996	0.001	0.015	0.988	0.003	0.023
	Air velocity: 7 (m/s)								
Wang and Singh	0.983	0.004	0.039	0.973	0.007	0.042	0.987	0.003	0.026
Henderson and Pabis	0.972	0.007	0.044	0.951	0.013	0.051	0.959	0.011	0.043
Logarithmic	0.993	0.002	0.025	0.989	0.003	0.026	0.997	0.001	0.013
Approximation of diffusion	**0.998**	**0.001**	**0.013**	**0.999**	**0.000**	**0.006**	**0.999**	**0.000**	**0.008**
Page	0.998	0.001	0.012	0.999	0.000	0.008	0.997	0.001	0.011
Two-term	0.998	0.001	0.015	0.999	0.000	0.007	0.999	0.000	0.009
Newton	0.962	0.010	0.045	0.925	0.019	0.057	0.937	0.017	0.050
Simplified Fick's diffusion	0.972	0.008	0.050	0.951	0.013	0.056	0.959	0.011	0.048
Modified Page equation-II	0.998	0.001	0.017	0.999	0.000	0.010	0.997	0.001	0.014
Midilli and Kucuk	0.998	0.001	0.016	0.999	0.000	0.008	0.998	0.001	0.011
	Air velocity: 8 (m/s)								
Wang and Singh	0.990	0.002	0.033	0.983	0.005	0.034	0.986	0.004	0.032
Henderson and Pabis	0.954	0.010	0.058	0.913	0.024	0.070	0.945	0.016	0.056
Logarithmic	0.998	0.001	0.016	0.999	0.000	0.009	0.998	0.001	0.011
Approximation of diffusion	**0.998**	**0.001**	**0.016**	**0.999**	**0.000**	**0.009**	**0.999**	**0.000**	**0.008**
Page	0.995	0.001	0.019	0.992	0.002	0.020	0.996	0.001	0.014
Two-term	0.998	0.001	0.022	0.999	0.000	0.010	0.999	0.000	0.009
Newton	0.944	0.012	0.056	0.879	0.034	0.075	0.923	0.022	0.061
Simplified Fick's diffusion	0.954	0.010	0.071	0.913	0.024	0.078	0.945	0.016	0.063
Modified Page equation-II	0.995	0.001	0.034	0.992	0.002	0.026	0.996	0.001	0.019
Midilli and Kucuk	0.997	0.001	0.025	0.999	0.000	0.009	0.999	0.000	0.009
	Air velocity: 9 (m/s)								
Wang and Singh	0.956	0.010	0.072	0.957	0.010	0.059	0.981	0.004	0.037
Henderson and Pabis	0.882	0.028	0.096	0.886	0.027	0.083	0.906	0.021	0.072
Logarithmic	0.994	0.001	0.026	0.993	0.002	0.024	0.999	0.000	0.007

Approximation of diffusion	**0.999**	**0.000**	**0.008**	**0.999**	**0.000**	**0.006**	**0.999**	**0.000**	**0.003**
Page	0.999	0.000	0.008	0.999	0.000	0.006	0.996	0.001	0.014
Two-term	0.999	0.000	0.011	0.999	0.000	0.008	0.988	0.003	0.037
Newton	0.852	0.035	0.093	0.842	0.038	0.087	0.871	0.028	0.075
Simplified Fick's diffusion	0.882	0.028	0.117	0.886	0.027	0.095	0.906	0.021	0.083
Modified Page equation-II	0.999	0.000	0.014	0.999	0.000	0.008	0.996	0.001	0.020
Midilli and Kucuk	0.999	0.000	0.014	0.999	0.000	0.008	0.976	0.005	0.052

As can be seen, in all of the evaluated conditions, "Approximation of diffusion" and "Two-term" models have the best results for fitting the moisture ratio curves. As shown, the highest R^2 values are obtained in the case of the Approximation of diffusion model. The values of the constant coefficients for the superior model at different drying conditions are presented in Table 4.

Comparison of experimental data and predicted data on the variation of moisture ratio with time at drying temperatures of 35 ºC, 45 ºC and 55 ºC is shown in Fig. 3, Fig. 4 and Fig. 5, respectively. It is observed that the experimental data and predicts data were close together. This shows that the selected model (Approximation of diffusion) predicts the experimental data successfully. For the case of mathematical modeling of paddy drying in a semi-industrial continuous band microwave dryer, Jafari et al. [19] reported that Wang and Page models, Lewis model, and Wang model had the best performance for fitting the drying curves of paddy grains at layer thicknesses of 6 mm, 12 mm and 18 mm, respectively. Nosrati et al. [20] showed that the moisture ratio curves in a hybrid infrared dryer during the drying process of rice grains could be appropriately presented by Page and Verma univariate models. In modeling and Optimizing drying variables in thin layer drying of parboiled paddy, Rao et al. [29] reported that the power model and the Arrhenius model had a good ability to fit the drying rate constant.

Table 4. Coefficients of "Approximation of diffusion" model for prediction of paddy grains moisture ratio in different drying conditions

	Gate angle	*0*			*45*			*90*		
Temperature (ºC)	Velocity (m/s)	a	b	k	a	b	k	a	b	k
35	7	0.3172	0.0491	0.0391	0.2741	0.0312	0.0647	0.2487	0.0439	0.0472
	8	0.3201	0.0381	0.0617	0.3200	0.0381	0.0617	0.2907	0.0248	0.0841
	9	0.3211	0.0283	0.0869	0.2818	0.0288	0.0843	0.2981	0.0265	0.0821
45	7	0.3466	0.0512	0.0596	0.2210	0.0462	0.0880	0.1873	0.0459	0.0866
	8	0.2439	0.0059	0.7513	0.2417	0.0438	0.0900	0.9974	0.0006	0.0095
	9	0.3005	0.0742	0.0647	0.2608	0.0526	0.0788	0.2090	0.0463	0.0929
55	7	0.2016	0.0971	0.1072	0.6188	0.0290	0.3675	0.3089	0.1064	0.0462
	8	0.5130	0.0664	0.0518	0.5629	0.0290	0.0427	0.4513	0.0911	0.0464
	9	0.3910	0.0504	0.1390	0.5680	0.0604	0.4267	0.4631	0.0463	0.0589

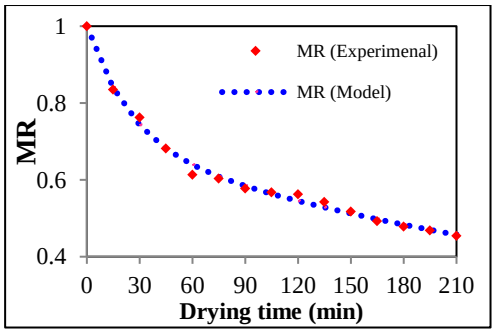

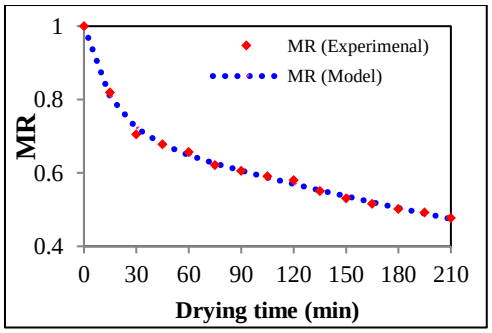

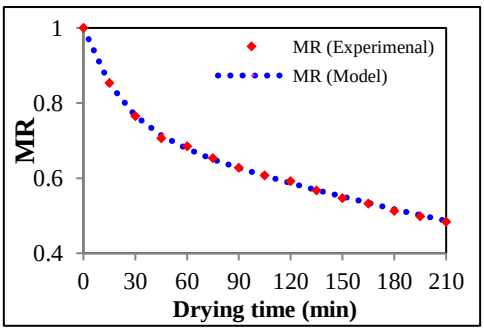

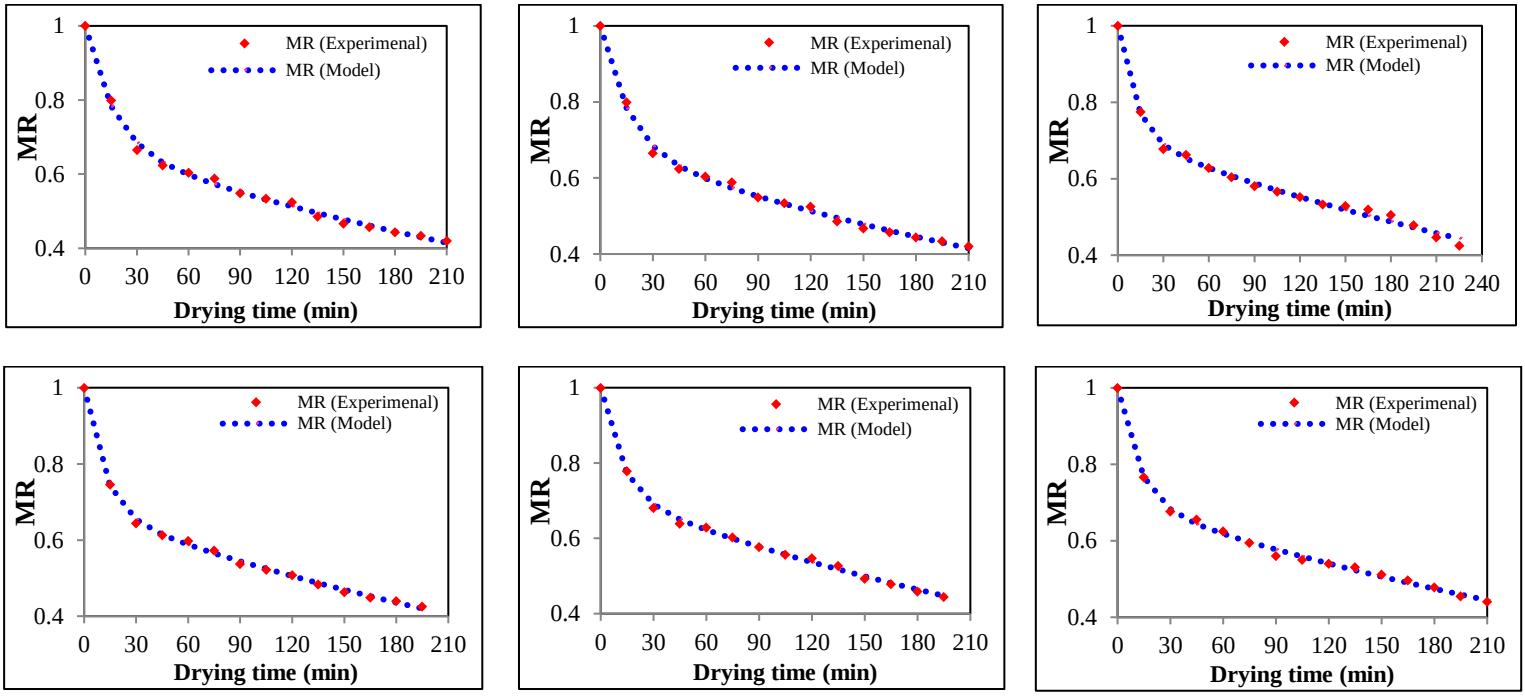

Fig 3. Variation of moisture ratio with time at drying temperature of 35 ºC.
In each row, the first, second and third charts represent gate angles of 0, 45 and 90 degrees, respectively.
In each column, the first, second and third charts represent drying air velocities of 7, 8 and 9 m/s, respectively.

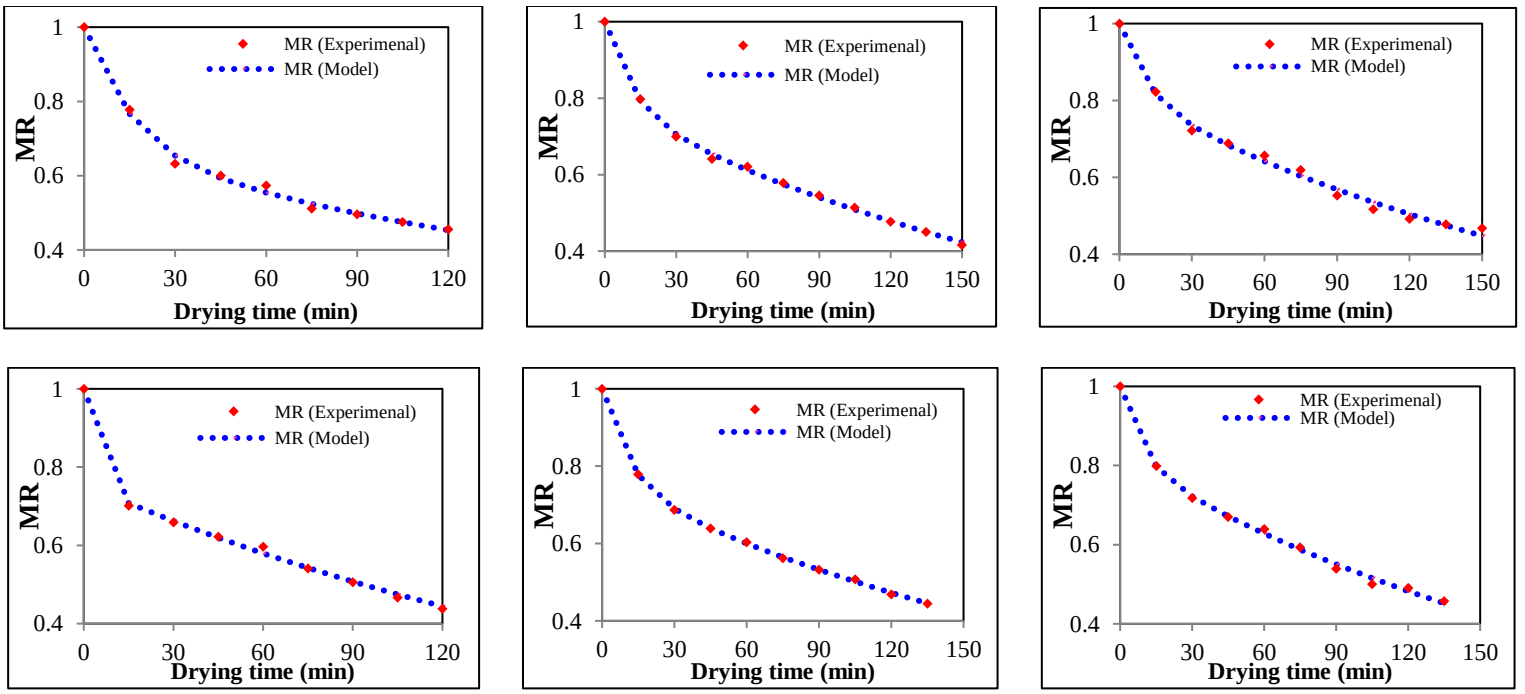

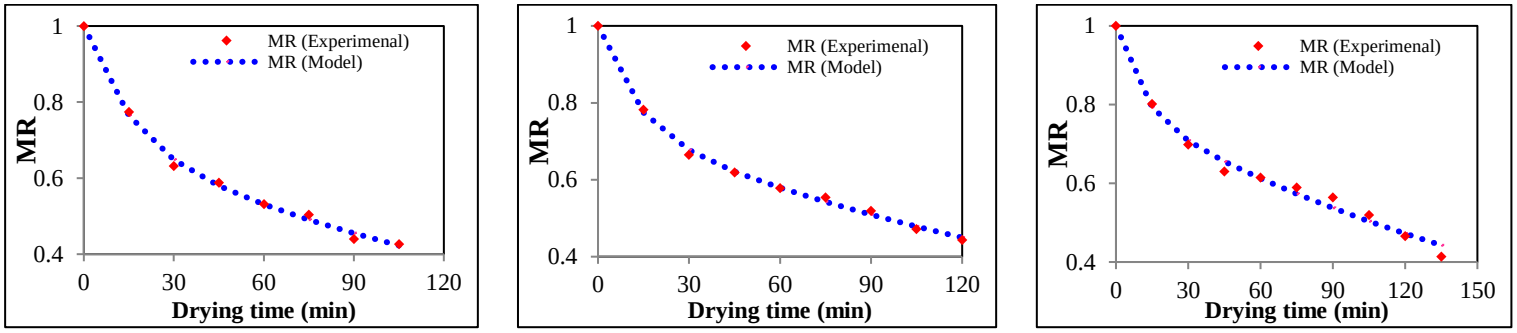

Fig 4. Variation of moisture ratio with time at drying temperature of 45 ºC. In each row, the first, second and third charts represent gate angles of 0, 45 and 90 degrees, respectively. In each column, the first, second and third charts represent drying air velocities of 7, 8 and 9 m/s, respectively.

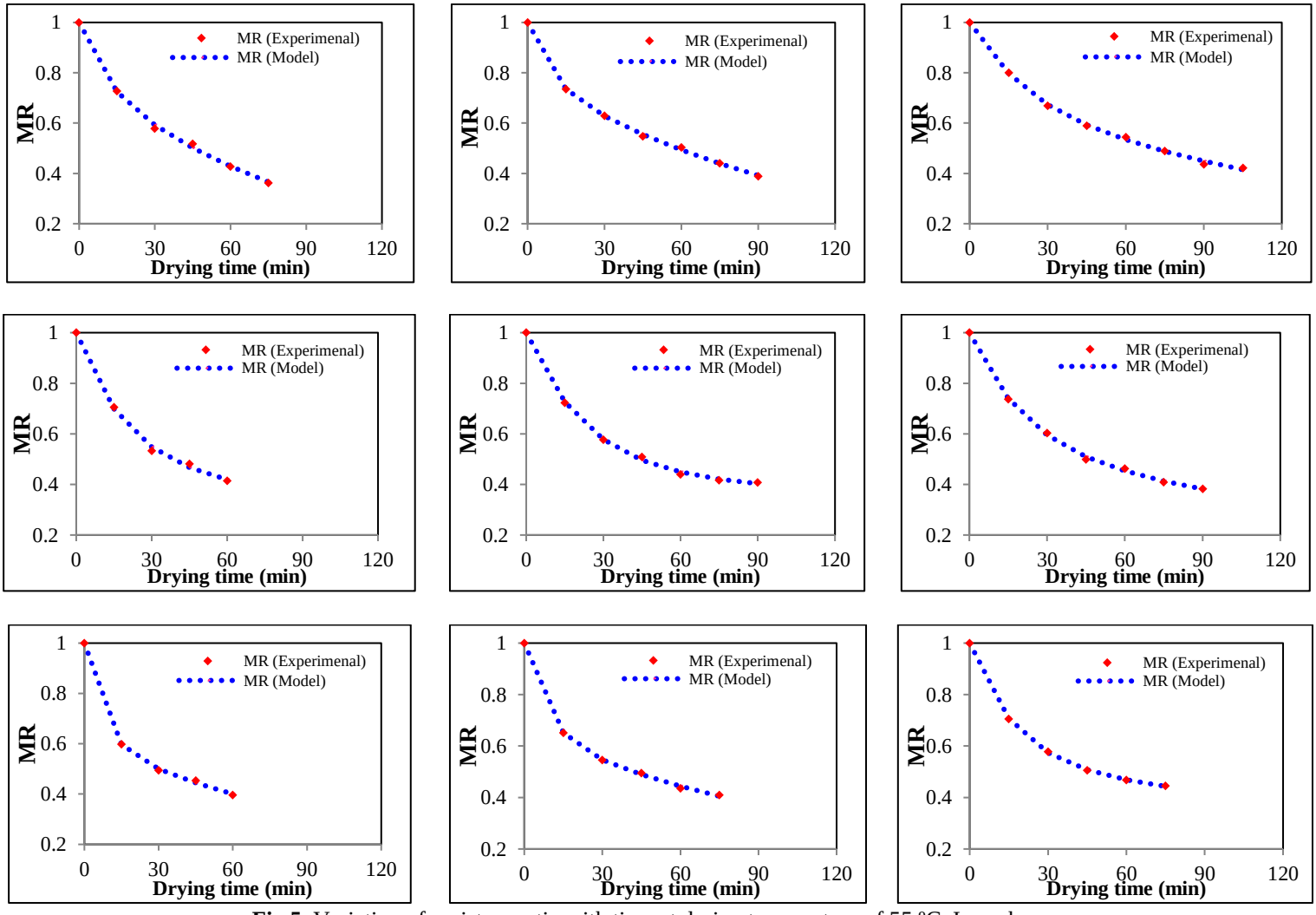

Fig 5. Variation of moisture ratio with time at drying temperature of 55 ºC. In each row, the first, second and third charts represent gate angles of 0, 45 and 90 degrees, respectively. In each column, the first, second and third charts represent drying air velocities of 7, 8 and 9 m/s, respectively.

3.3. Analytical modeling

The required treatments for conducting the experiments were defined using response surface methodology (RSM). The statistical analysis of the models was done using Box–Behnken design method. The design points suggested by Box–Behnken method for conducting the experiments and their related experimental data are given in Table 5. As shown, three experimental factors, namely drying air temperature, drying air velocity and angle of desiccant regeneration gate with respect to four responses, including drying time, total energy consumption, solar energy fraction and energy efficiency, were modeled using the Box-Behncken method. Based on the software analysis, 19 run points were defined considering the different combinations of experimental factors. The variance analysis indicated that for all of the four responses, including drying time, total energy consumption, solar fraction and energy efficiency, the quadratic model could successfully and significantly fit the performance characteristics of the drying system.

The fit summary of the model responses is given in Table 6. The high adjusted R^2 values indicated the suitability of the developed models. The predicted R^2 values were close to the adjusted R^2 values. The related F-values of the developed model implied its significance.

The variance analysis indicated that for Quadratic model regarding the four responses are shown in Table 7. It can be seen that the suggested model was significant for all of the four evaluated responses. P-values less than 0.0500 indicate model terms are significant. In this case, A, B, C, AB, B^2, C^2 are significant model terms. Values greater than 0.1000 indicate the model terms are not significant. If there are many insignificant model terms (not counting those required to support hierarchy), model reduction may improve the model.

Table 5. The design points suggested by Box–Behnken method for conducting the experiments and their related experimental data.

Std	Run	Factor 1: Air velocity (m/s)	Factor 2: Air temperature (ºC)	Factor 3: Gate angle (degree)	Response 1: Drying time (min)	Response 2: Total energy consumption (kWh)	Response 3: Solar Fraction (Dimensionless)	Response 4: Energy efficiency (%)
2	1	9	35	0	171	0.6019	0.3508	27.22
6	2	9	35	90	196	0.6899	0.3711	23.07
5	3	7	35	90	245	0.6502	0.2444	24.50
8	4	9	55	90	78	0.8015	0.3209	19.42
4	5	9	55	0	54	0.5149	0.4857	30.26
13	6	8	45	0	106	0.3292	0.5260	47.67
17	7	8	45	45	128	0.3882	0.5160	40.44
12	8	8	55	45	81	0.6251	0.3798	25.18
19	9	8	45	45	130	0.3790	0.5080	41.04
15	10	8	45	45	128	0.3910	0.5150	40.91
16	11	8	45	45	125	0.3740	0.5096	39.78
7	12	7	55	90	98	0.5171	0.4385	30.13
18	13	8	45	45	129	0.3846	0.5163	41.84
14	14	8	45	90	131	0.4069	0.5359	38.47
11	15	8	35	45	214	0.6567	0.3034	24.65
1	16	7	35	0	216	0.5732	0.1793	27.30
3	17	7	55	0	68	0.3554	0.5135	44.77
9	18	7	45	45	141	0.3788	0.5079	41.97
10	19	9	45	45	112	0.3989	0.5043	40.00

Table 6. Statistical analysis of the applied models for responses fitting.

Source	Sequential p-value	Lack of fit p-value	Adjusted R^2	Predicted R^2	Comments
Drying time (min)					
Linear	< 0.0001	0.0009	0.9526	0.9303	
2FI	0.3459	0.0008	0.9545	0.8775	
Quadratic	**< 0.0001**	**0.6234**	**0.9989**	**0.9980**	**Suggested**
Cubic	0.8422	0.2184	0.9985	0.8066	Aliased
Total energy consumption (kWh)					
Linear	0.2191	< 0.0001	0.0984	-0.2792	
2FI	0.6876	< 0.0001	-0.0012	-2.2985	
Quadratic	**< 0.0001**	**0.0014**	**0.9411**	**0.7096**	**Suggested**
Cubic	0.0081	0.0160	0.9904	-1.7810	Aliased
Solar Fraction (Dimensionless)					
Linear	0.2316	< 0.0001	0.0906	-0.3864	
2FI	0.3155	< 0.0001	0.1443	-2.0234	
Quadratic	**< 0.0001**	**0.0008**	**0.9592**	**0.8241**	**Suggested**
Cubic	0.0003	0.1622	0.9982	0.7320	Aliased
Energy Efficiency (%)					
Linear	0.2640	< 0.0001	0.0719	-0.3161	
2FI	0.6993	< 0.0001	-0.0348	-2.3697	
Quadratic	**< 0.0001**	**0.0321**	**0.9622**	**0.8260**	**Suggested**
Cubic	0.0115	0.4591	0.9929	0.6291	Aliased

Table 7. Variance analysis of Quadratic model for drying time, total energy consumption, solar fraction and energy efficiency.

Source	Sum of squares	df	Mean Square	F-value	p-value
Drying time (min)					
Model	50146.44	9	5571.83	1840.34	< 0.0001
A-air velocity	2464.90	1	2464.90	814.14	< 0.0001
B-air temperature	43956.90	1	43956.90	14518.70	< 0.0001
C-angle	1768.90	1	1768.90	584.26	< 0.0001
AB	450.00	1	450.00	148.63	< 0.0001
AC	12.50	1	12.50	4.13	0.0727
BC	0.0000	1	0.0000	0.0000	1.0000
A^2	0.0163	1	0.0163	0.0054	0.9431
B^2	1213.88	1	1213.88	400.94	< 0.0001
C^2	171.51	1	171.51	56.65	< 0.0001
Residual	27.25	9	3.03		
Total energy consumption					
Model	0.3470	9	0.0386	32.97	< 0.0001
A-air velocity	0.0284	1	0.0284	24.25	0.0008
B-air temperature	0.0128	1	0.0128	10.95	0.0091
C-angle	0.0477	1	0.0477	40.82	0.0001
AB	0.0176	1	0.0176	15.08	0.0037
AC	0.0023	1	0.0023	1.97	0.1937
BC	0.0100	1	0.0100	8.58	0.0168
A^2	0.0003	1	0.0003	0.2574	0.6241
B^2	0.1595	1	0.1595	136.33	< 0.0001
C^2	0.0027	1	0.0027	2.29	0.1647
Residual	0.3470	9	0.0386	32.97	< 0.0001
Solar Fraction (Dimensionless)					
Model	0.2096	9	0.0233	48.06	< 0.0001
A-air velocity	0.0022	1	0.0022	4.59	0.0607
B-air temperature	0.0475	1	0.0475	98.04	< 0.0001

C-angle	0.0021	1	0.0021	4.30	0.0679
AB	0.0246	1	0.0246	50.75	< 0.0001
AC	0.0023	1	0.0023	4.67	0.0590
BC	0.0132	1	0.0132	27.29	0.0005
A^2	0.0000	1	0.0000	0.0521	0.8245
B^2	0.0767	1	0.0767	158.29	< 0.0001
C^2	0.0013	1	0.0013	2.68	0.1361
Residual	0.0044	9	0.0005		
Energy efficiency (%)					
Model	1337.40	9	148.60	51.97	< 0.0001
A-air velocity	82.38	1	82.38	28.81	0.0005
B-air temperature	53.04	1	53.04	18.55	0.0020
C-angle	173.43	1	173.43	60.65	< 0.0001
AB	70.20	1	70.20	24.55	0.0008
AC	0.7548	1	0.7548	0.2640	0.6198
BC	42.95	1	42.95	15.02	0.0038
A^2	0.7931	1	0.7931	0.2774	0.6112
B^2	658.66	1	658.66	230.34	< 0.0001
C^2	18.85	1	18.85	6.59	0.0303
Residual	25.74	9	2.86		

In the following, the mathematical equations related to the four responses are given based on the effective factors and their interactions. The equation in terms of coded factors can be used to make predictions about the response for given levels of each factor. By default, the high levels of the factors are coded as +1, and the low levels are coded as -1. The coded equation is useful for identifying the relative impact of the factors by comparing the factor coefficients. Thus

$$\begin{aligned} Drying\ time = {} & 127.30 - 15.70(A) \\ & - 66.30(B) \\ & + 13.30(C) \\ & + 7.50(AB) \\ & - 1.25(AC) \\ & + 0.0000(BC) \\ & - 0.0773(A^2) \\ & + 21.08(B^2) \\ & - 7.92(C^2), \end{aligned} \quad (15)$$

$$\begin{aligned} Total\ energy\ consumption & \\ = {} & 0.3905 \\ & + 0.0533(A) \\ & - 0.0358(B) \\ & + 0.0691(C) \\ & + 0.0470(AB) \\ & + 0.0170(AC) \\ & + 0.0354(BC) \\ & - 0.0105(A^2) \\ & + 0.2416(B^2) \\ & - 0.0313(C^2), \end{aligned} \quad (16)$$

$$\begin{aligned} Solar\ fraction = {} & 0.5113 \\ & + 0.0149(A) \\ & + 0.0689(B) \\ & - 0.0144(C) \\ & - 0.0554(AB) \\ & - 0.0168(AC) \\ & - 0.0407(BC) \\ & - 0.0030(A^2) \\ & - 0.1675(B^2) \\ & + 0.0218(C^2)\ and \end{aligned} \quad (17)$$

$$\begin{aligned} Energy\ efficiency = {} & 40.64 - \\ & 2.87(A) + 2.30(B) - 4.16(C) - \\ & 2.96(AB) + 0.3072(AC) - \\ & 2.32(BC) + 0.5388(A^2) - \\ & 15.53(B^2) + 2.63(C^2). \end{aligned} \quad (18)$$

The variations of four responses with respect to each factor are illustrated in Fig. 6. As can be seen in Fig. 6a, with increasing the air velocity, drying time decreases gradually. Increasing the air temperature had a stronger effect, and it caused the drying time to increase with a higher slope.

The highest value of drying time was equal to 245 minutes obtained at a drying air temperature of 35 °C, drying air velocity of 7 m/s, and a regeneration gate angle of 90. The lowest drying time (68 minutes) was attributed to the drying air temperature of 55 °C, air velocity of 7 m/s, and a regeneration gate angle of 0. Similar results have been reported concerning the influence of drying air temperature on water chestnut rehydration [49]. Increasing the inlet air velocity from 7

to 9 m/s resulted in reduced product drying time. In accordance, other studies have reported that increased inlet air velocity leads to decreased drying time [50-52]. Rao et al. [12] reported that the optimum process parameters to gain minimum specific energy and minimum drying time included air velocity of 0.55–0.68 m/s and drying air temperature of 112–116 ºC. The mentioned combination resulted in specific energy consumption of 8.5–10.7 MJ/kg of water removed.

The effect of air temperature and air velocity on the total energy consumption is shown in Fig. 6b. It can be seen that the system total energy consumption at 35 °C drying temperature was higher than that of 45 °C, and those values of 55 °C temperature were greater than 45 °C temperature. This is due to the fact that at lower drying temperatures, the drive motors of the desiccant wheel mechanism and centrifugal fan worked for a longer time. According to the points suggested by RSM, the highest value of the total energy consumption (0.8015 kWh) was obtained at drying air temperature of 55 °C, drying air velocity of 9 m/s, and regeneration gate angle of 90. It should be noted that the angles of 0, 45 and 90 degrees represent "Closed", "Semi-open", and "Open" status of the desiccant regeneration gate, respectively. The lowest value of the system's total energy consumption was equal to 0.3292 kWh, which was obtained at drying air temperature of 45 °C, air velocity of 8 m/s, and "closed" status of the return air gate. These values were obtained from the three main energy-consuming parts of the drying system, including the gas water heater, centrifugal fan, and desiccant wheel. At two levels of drying air temperatures (35 °C and 45 °C), the gas water heater was not applied in the drying process, and the required thermal energy during the drying process was supplied only by the solar water heater.

Regarding the angle of the desiccant regeneration gate, the highest energy consumption of the drying system was related to "90, 45 and 0 degrees, respectively. Increasing the drying air velocity caused the total energy consumption of the drying system to increase. Similar results have been reported by Nazgelichi et al. [17] and Nassiri and Etesami [18]. Jafari et al. [19] reported that energy efficiency and exergy efficiency increased by increasing grain layers' thickness in a continuous band microwave paddy dryer. When the layers' thicknesses were the same, the energy efficiency and exergy efficiency decreased with increasing microwave power. Elhami et al. [23] found that the ANFIS model could better predict the energy output and benefit-cost ratio than the linear regression model. The energy use efficiency was equal to 0.9 and 1.02 for lentils and chickpea, respectively, while the benefit-cost ratio was obtained at 1.60 for lentil and 1.74 for chickpea.

Solar fraction represents the part of system energy consumption that was provided by solar energy. The solar energy was provided in two forms: a) thermal energy by solar water heater to supply the drying air; and b) electrical energy by solar panels to drive the drive motor of desiccant mechanism. As shown in Fig. 6c, the highest solar fraction values belong to the drying air temperature of 45 °C. At 35 °C temperature level, although a considerable part of the required hot air could be supplied by the solar water heater, however, because of a longer working duration of the centrifugal fan, the solar fraction in the drying system reduces. Increasing the air velocity caused the solar fraction to increase.

The highest solar fraction during the drying process (0.5359) was obtained at a drying air temperature of 45 °C, drying air velocity of 8 m/s, and regeneration gate angle of 90. The lowest value of solar fraction (0.1793) was attributed to the drying air temperature of 35 °C, air velocity of 7 m/s, regeneration gate angle of 0. Ziaforoughi and Esfahani [15] examined the energy consumption in the potato drying process using a photovoltaic-solar collector-assisted intermittent infrared dryer. They reported by using their developed solar system, the amount of electric energy consumption and product drying time reduced by 40-69% and 31-52% compared to nonrenewable infrared lightning.

Fig. 6d indicates that the highest energy efficiency of the drying system occurs at a

drying temperature of 45 ºC. This means that at this level of temperature, most of the system energy is being used effectively for the product dehydration. The highest energy efficiency value was equal to 50.36%, obtained at a drying temperature of 45 °C, air velocity of 7 m/s and gate angle of 0 degree. Meanwhile, the lowest energy efficiency (19.42 %) was attributed to the drying air temperature of 55 °C, air velocity of 9 m/s and a gate angle of 90 degrees. Jafari et al. [19] reported that energy efficiency and exergy efficiency increased by increasing the thickness of grain layers in a continuous band microwave paddy dryer. When the layers' thicknesses were the same, the energy efficiency and exergy efficiency decreased with increasing microwave power. Sarker et al. [27] reported that the exergy efficiency for an industrial non-solar fluidized bed paddy dryer at different working conditions varied from 46.99 to 58.14%. The solar-assisted dryer proposed in this study can satisfactorily compete with the commercial-scale dryers.

The relation between the actual (experimental) and predicted (model) data regarding the four performance characteristics of the proposed hybrid solar dryer is presented in Fig. 7. It can be observed that for all of the responses, there was a good agreement between the actual and predicted data.

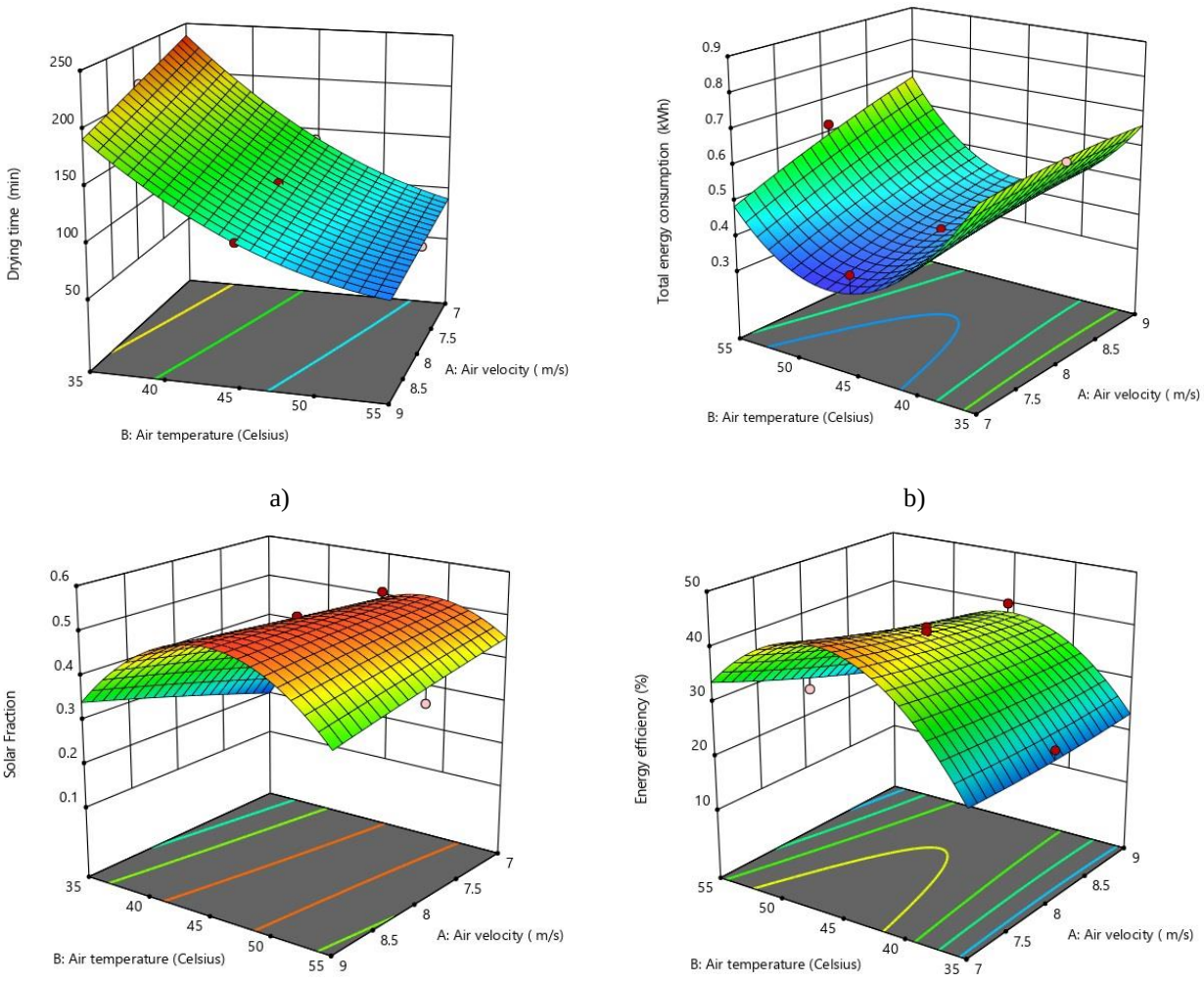

Fig. 6. The effect of drying air temperature and air velocity on a) drying time, b) energy consumption, and c) solar fraction of fluidized-bed paddy drying system.

3.4. Optimization

The performance of the drying system was optimized according to three working factors (drying air temperature, drying air velocity and angle of desiccant regeneration gate). The objective of the optimization process was to minimize drying time and total energy consumption and to maximize the solar energy fraction. The optimal values for the evaluated factors were obtained using the desirability function method. The results revealed that 41 points could be suggested with high desirability levels (at least 0.917). The top 10 solutions are given in Table 8. The graphical view of the optimum point is given in Fig. 8. As shown, by applying the suggested point, a considerable share of solar energy together with lower levels of energy consumption and drying time is achievable. The selected optimum point included drying air velocity of 7 m/s, drying air temperature of 52.77 ºC and regeneration gate angle of 0. Under the mentioned working conditions, the drying time of 75.99 min, the total energy consumption of 0.297 kWh, solar energy fraction of 0.540 and energy efficiency of 47.67% could be obtained. Gharnasi Gharavi et al. [21] reported that RSM could be successfully applied to develop appropriate prediction models for describing the paddy drying process. They showed that changes in the quality parameters were adequately described by the quadratic model.

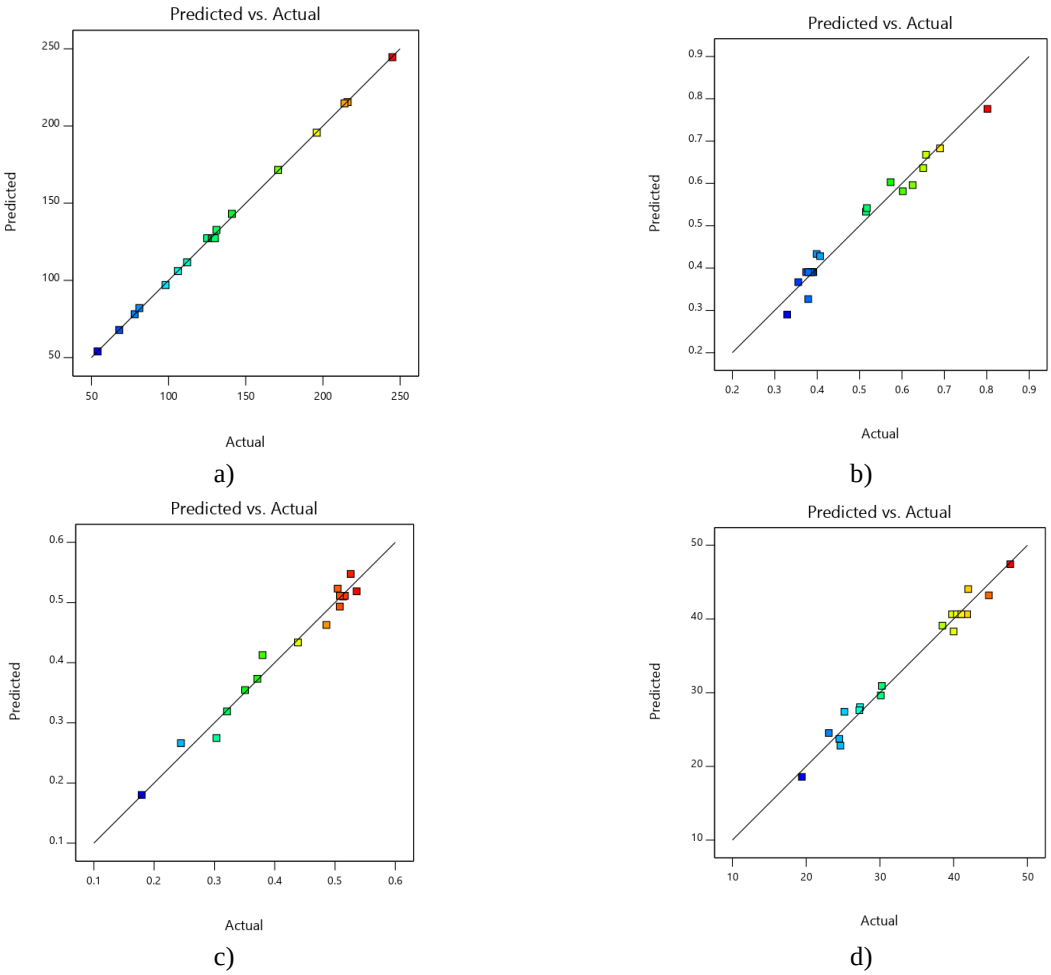

Fig. 7. Optimization charts of the solar-assisted fluidized-bed paddy drying system considering performance characteristics including a) drying time, b) total energy consumption, c) solar energy fraction, and d) desirability of the optimum point.

According to the optimization process, the minimum losses (percentage of breakage and percentage of the crack) and drying time were found with the inlet air temperature 56.53 °C, the cylinder rotation speed of 10 rpm and the cylinder fullness of 54.20%. Shirinbakhsh and Amidpour [16] reported that drying biomass using their proposed dryer costs between 4 and 7 cents per kilogram of biomass and under optimum economic conditions, the solar fraction is less than 6%. The solar fraction could be increased to more than 55% by ignoring economic constraints and reducing the dryer's capacity. Pourbagher et al. [53] indicated that the quadratic model successfully fit the experimental data in the infrared fluidized bed dryer. Based on the genetic algorithm approach, the optimized condition included air temperatures of 55.25°C and 58°C for Tarom and Shirudi varieties, respectively

Table 8. The optimal working conditions for the studied solar-assisted fluidized-bed paddy dryer.

No.	Drying air velocity (m/s)	Drying air temperature (°C)	Gate angle (°)	Drying time (min)	Total energy consumption (kWh)	Solar fraction	Energy efficiency (%)	Desirability	
1	**7.000**	**52.769**	**0.000**	**75.991**	**0.297**	**0.540**	**47.670**	**0.970**	**Selected**
2	7.007	52.740	0.001	76.046	0.297	0.540	47.670	0.970	
3	7.035	52.632	0.000	76.251	0.297	0.541	47.670	0.970	
4	7.000	52.688	0.000	76.324	0.295	0.541	47.803	0.969	
5	7.049	52.576	0.001	76.360	0.297	0.541	47.670	0.969	
6	7.000	52.715	0.342	76.440	0.297	0.540	47.670	0.969	
7	7.000	52.714	0.353	76.454	0.297	0.540	47.670	0.969	
8	7.000	52.873	0.000	75.566	0.300	0.539	47.497	0.969	
9	7.087	52.420	0.000	76.661	0.297	0.543	47.671	0.969	
10	7.000	52.551	0.001	76.895	0.292	0.542	48.023	0.969	

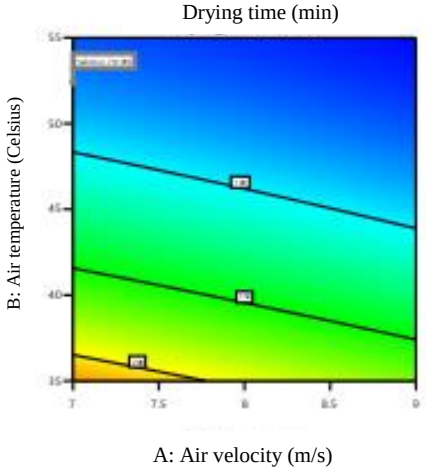

a)

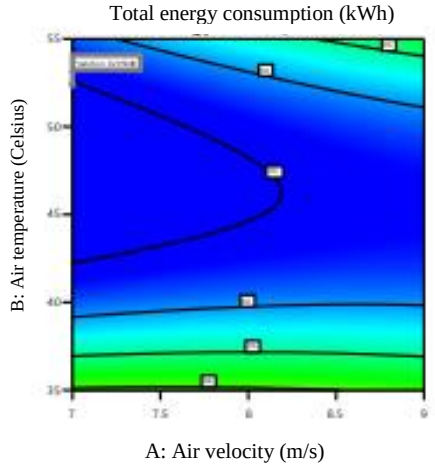

b)

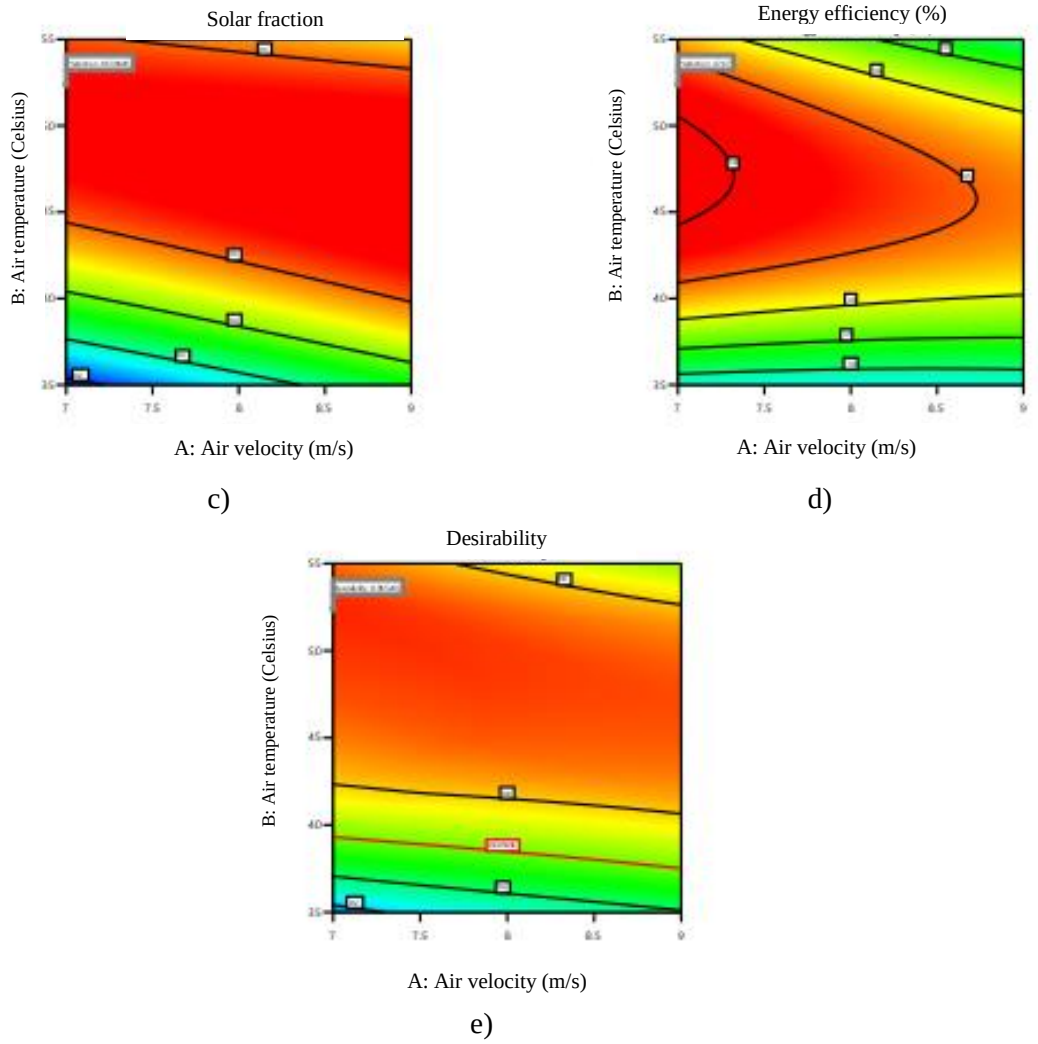

Fig. 8. The graphical view of the optimum point considering:
a) drying time, b) total energy consumption, c) solar energy fraction, and d) desirability of the optimum point.

Fig. 9. Contour of blade film cooling effectiveness for various time steps of a cycle of sinusoidal pulsation at frequency of 50 Hz and M=0.5

4. Conclusions

The objective of this study was to model and optimize the performance characteristics of a solar-assisted fluidized-bed paddy dryer. The major parts of the drying system included a solar water heater, a solar-powered infrared lamp, a gas water heater, and a desiccant wheel mechanism. The studied factors were drying air temperature, drying air velocity, and angle of desiccant regeneration gate. The core findings of the research are listed as follows:

- According to the points suggested by RSM, the highest value of the total energy consumption (0. 8015 kWh) was obtained at drying air temperature of 55 °C, drying air velocity of 8 m/s, and regeneration gate angle of 90. The lowest value of the system's total energy consumption was equal to 0. 3292 kWh, which was obtained at drying air temperature of 45 °C, air velocity of 7 m/s, and gate angle of 0.
- Applying higher levels of drying air velocity resulted in reduced product drying time. The highest and lowest drying time values (245 minutes and 68 minutes) were

obtained at drying air velocity of 7 and 8 m/s, respectively.

- The highest solar fraction during the drying process (0.5359) was obtained at a drying air temperature of 45 °C, drying air velocity of 7 m/s, and regeneration gate angle of 90. The lowest value of solar fraction (0. 1793) was attributed to the drying air temperature of 35 °C, air velocity of 7 m/s, regeneration gate angle of 45.
- Due to increased moisture release from the inside to the product surface at the initial stage of the drying process, the drying rate increased quickly. Later, the drying rate varied with low tolerances and reached its ultimate point in a lengthier time.
- With the increase of the drying air temperature, the drying rate curves were higher in their related chart. This was due to the fact that the drying process was done at higher speeds. Increasing the drying air velocity caused the drying rate to be increased. The drying rate decreased by increasing the angle of the desiccant regeneration gate.
- Several common mathematical models were applied to predict the paddy drying process in the hybrid solar dryer. According to the statistical analysis, the "Approximation of diffusion" model was selected as the best model to fit the moisture ratio curves with the highest R^2 and lowest χ^2 and RMSE values.
- Response Surface Methodology (RSM) based on the Box–Behnken technique was used. The variance analysis of the results showed that the quadratic model could successfully fit the performance characteristics of the drying system. The selected optimum point included drying air velocity of 7 m/s, drying air temperature of 52.77 ºC and regeneration gate angle of 0. Under the mentioned working conditions, the drying time of 75.99 min, the total energy consumption of 0.297 kWh, solar energy fraction of 0.540 and energy efficiency of 47.67% could be acquired.

Acknowledgment

The authors would like to thank the University of Guilan for providing the laboratory facilities for conducting this project. This research did not receive any specific grant from funding agencies in the public, commercial, or not-for-profit sectors.

References

[1] Noorpoor, A., et al., A thermodynamic model for exergetic performance and Optimization of a solar and biomass-fuelled multigeneration system. Energy Equipment and Systems, 2016. 4(2): p. 281-289.

[2] IME, Energy Balance Sheet. 2011, Iran Ministry of Energy: Tehran, Iran.

[3] Kumar, A., S. Chamoli, and M. Kumar, Experimental investigation on thermal performance and fluid flow characteristics in heat exchanger tube with solid, hollow circular disk inserts. Applied Thermal Engineering, 2016. 100: p. 227-236.

[4] Zareiforoush, H., et al., Design, development and performance evaluation of an automatic control system for rice whitening machine based on computer vision and fuzzy logic. Computers and Electronics in Agriculture, 2016. 124: p. 14-22.

[5] Gazor, H.R., M.R. Alizadeh, and M. Younesi Alamouti, Comparison of Operational Parameters and Energy Consumption in Rice Milling Systems (Case Study in Mazandaran Province). Journal of Engineering Research in Agricultural Mechanization and Systems, 2016. 17(66): p. 15-28.

[6] Li, H., et al., Characteristics of fluidisation behaviour in a pressurised bubbling fluidised bed. The Canadian Journal of Chemical Engineering, 2013. 91(4): p. 760-769.

[7] Senadeera, W., O. Alves-Filho, and T. Eikevik, Influence of drying conditions on the moisture diffusion and fluidization quality during multi-stage fluidized bed drying of bovine intestine for pet food. Food and Bioproducts Processing, 2013. 91(4): p. 549-557.

[8] Si, C., et al., Experimental and numerical simulation of drying of lignite in a microwave-assisted fluidized bed. Fuel, 2019. 242: p. 149-159.
[9] Yahya, M., Design and performance evaluation of a solar assisted heat pump dryer integrated with biomass furnace for red chili. International Journal of Photoenergy, 2016. 2016.
[10] Delele, M.A., F. Weigler, and J. Mellmann, Advances in the application of a rotary dryer for drying of agricultural products: A review. Drying technology, 2015. 33(5): p. 541-558.
[11] Eltawil, M.A., M.M. Azam, and A.O. Alghannam, Energy analysis of hybrid solar tunnel dryer with PV system and solar collector for drying mint (MenthaViridis). Journal of Cleaner Production, 2018. 181: p. 352-364.
[12] Hamdi, I., et al., Drying of red pepper slices in a solar greenhouse dryer and under open sun: Experimental and mathematical investigations. Innovative Food Science & Emerging Technologies, 2019.
[13] Karthikeyan, A. and S. Murugavelh, Thin layer drying kinetics and exergy analysis of turmeric (Curcuma longa) in a mixed mode forced convection solar tunnel dryer. Renewable Energy, 2018. 128: p. 305-312.
[14] Yahya, M., A. Fudholi, and K. Sopian, Energy and exergy analyses of solar-assisted fluidized bed drying integrated with biomass furnace. Renewable energy, 2017. 105: p. 22-29.
[15] Ziaforoughi, A. and J.A. Esfahani, A salient reduction of energy consumption and drying time in a novel PV-solar collector-assisted intermittent infrared dryer. Solar Energy, 2016. 136: p. 428-436.
[16] Shirinbakhsh, M. and M. Amidpour, Design and Optimization of solar-assisted conveyer-belt dryer for biomass. Energy Equipment and Systems, 2017. 5(2): p. 85-94.
[17] Nazghelichi, T., M.H. Kianmehr, and M. Aghbashlo, Thermodynamic analysis of fluidized bed drying of carrot cubes. Energy, 2010. 35(12): p. 4679-4684.
[18] Nassiri, S.M. and S.M. Etesami, Energy Use Efficiency of Different Drying Methods for Two Rough Rice Cultivars. Food Science and Technology, 2015. 3(2): p. 23-28.
[19] Jafari, H., D. Kalantari, and M. Azadbakht, Semi-industrial continuous band microwave dryer for energy and exergy analyses, mathematical modeling of paddy drying and it's qualitative study. Energy, 2017. 138: p. 1016-1029.
[20] Nosrati, M., et al., Modeling and Optimization of Rough Rice Drying under Hot Air-Infrared Radiation in a Laboratory Scale Vibratory Bed Dryer. Int. J. Biomed. Sci. Eng, 2018. 49: p. 423-435.
[21] Gharnasi Gharavi, O., et al., Optimization of paddy rice drying using response surface methodology. Electronic Journal of Food Processing and Preservation, 2017. 10(1): p. 99-116.
[22] Pourbagher, R., et al., Modeling and Optimization of drying process of paddy in infrared and warm air fluidized bed dryer. Agricultural Engineering International: CIGR Journal, 2018. 20(3): p. 162-171.
[23] Elhami, B., et al., Application of ANFIS and linear regression models to analyze the energy and economics of lentil and chickpea production in Iran. Energy Equipment and Systems, 2016. 4(2): p. 255-270.
[24] Sarker, M., et al., application of simulation in determining suitable operating parameters for industrial scale fluidized bed dryer during drying of high impurity moist paddy. Journal of Stored Products Research, 2015. 61: p. 76-84.
[25] Zomorodian, A., D. Zare, and H. Ghasemkhani, Optimization and evaluation of a semi-continuous solar dryer for cereals (Rice, etc.). Desalination, 2007. 209(1-3): p. 129-135.
[26] Golmohammadi, M., et al., Energy efficiency investigation of intermittent paddy rice dryer: Modeling and experimental study. Food and bioproducts processing, 2015. 94: p. 275-283.

[27] Sarker, M.S.H., et al., Energy and exergy analysis of industrial fluidized bed drying of paddy. Energy, 2015. 84: p. 131-138.
[28] Atthajariyakul, S. and T. Leephakpreeda, Fluidized bed paddy drying in optimal conditions via adaptive fuzzy logic control. Journal of food engineering, 2006. 75(1): p. 104-114.
[29] Rao, P.S., S. Bal, and T. Goswami, Modelling and Optimization of drying variables in thin layer drying of parboiled paddy. Journal of Food Engineering, 2007. 78(2): p. 480-487.
[30] Behera, G. and P. Sutar, A comprehensive review of mathematical modeling of paddy parboiling and drying: Effects of modern techniques on process kinetics and rice quality. Trends in Food Science & Technology, 2018. 75: p. 206-230.
[31] ASABE, Moisture Measurement—Unground Grain and Seeds. 2019, American Society of Agricultural and Biological Engineers.
[32] Labed, A., et al., Solar drying of henna (Lawsonia inermis) using different models of solar flat plate collectors: an experimental investigation in the region of Biskra (Algeria). Journal of Cleaner Production, 2016. 112: p. 2545-2552.
[33]Doymaz, Effect of citric acid and blanching pre-treatments on drying and rehydration of Amasya red apples. Food and Bioproducts Processing, 2010. 88(2-3): p. 124-132.
[34]Balbay, A. and Ö. Şahin, Microwave drying kinetics of a thin-layer liquorice root. Drying Technology, 2012. 30(8): p. 859-864.
[35]Tohidi, M., M. Sadeghi, and M. Torki-Harchegani, Energy and quality aspects for fixed deep bed drying of paddy. Renewable and Sustainable Energy Reviews, 2017. 70: p. 519-528.
[36]Firouzi, S., M.R. Alizadeh, and D. Haghtalab, Energy consumption and rice milling quality upon drying paddy with a newly-designed horizontal rotary dryer. Energy, 2017. 119: p. 629-636.
[37]Sharifi, H., Babapour, Sh., Sherkati, Sh., Evaluation of Problems Caused By Thermal Degradation of Consumed Gas in Iran's Thermal Power Stations, in 18th International Conference of Electronics. 2004: Tehran, Iran.
[38]Duffie, J.A. and W.A. Beckman, Solar engineering of thermal processes. 2013: John Wiley & Sons.
[39]Doymaz, I., Convective air drying characteristics of thin layer carrots. Journal of food engineering, 2004. 61(3): p. 359-364.
[40]Minaei, S., et al., Mathematical models of drying pomegranate arils in vacuum and microwave dryers. 2012.
[41] Akpinar, E.K., Drying of mint leaves in a solar dryer and under open sun: modelling, performance analyses. Energy conversion and management, 2010. 51(12): p. 2407-2418.
[42]Erenturk, S., M. Gulaboglu, and S. Gultekin, The thin-layer drying characteristics of rosehip. Biosystems Engineering, 2004. 89(2): p. 159-166.
[43]Torki-Harchegani, M., et al., Dehydration behaviour, mathematical modeling, energy efficiency and essential oil yield of peppermint leaves undergoing microwave and hot air treatments. Renewable and Sustainable Energy Reviews, 2016. 58: p. 407-418.
[44]Özbek, B. and G. Dadali, Thin-layer drying characteristics and modeling of mint leaves undergoing microwave treatment. Journal of Food Engineering, 2007. 83(4): p. 541-549.
[45]Myers, R.H., D.C. Montgomery, and C.M. Anderson-Cook, Response surface methodology: process and product optimization using designed experiments. 2016: John Wiley & Sons.
[46]Mghazli, S., et al., Drying characteristics and kinetics solar drying of Moroccan rosemary leaves. Renewable Energy, 2017. 108: p. 303-310.
[47]Spence, J., et al., Investigation into thin layer drying rates and equilibrium moisture content of abattoir paunch waste. Renewable Energy, 2018. 124: p. 95-102.
[48]Kingsly, R.P., et al., Effects of pretreatments and drying air temperature on drying behaviour of peach slice.

International journal of food science & technology, 2007. 42(1): p. 65-69.
[49]Akbulut, A. and A. Durmuş, Thin layer solar drying and mathematical modeling of mulberry. International journal of energy research, 2009. 33(7): p. 687-695.
[50]Singh, G.D., et al., Drying and rehydration characteristics of water chestnut (Trapa natans) as a function of drying air temperature. Journal of Food Engineering, 2008. 87(2): p. 213-221.
[51]Benseddik, A., et al., Mathematical empirical models of thin-layer airflow drying kinetics of pumpkin slice. Engineering in Agriculture, Environment and Food, 2018. 11(4): p. 220-231.
[52]Ndukwu, M.C., Effect of drying temperature and drying air velocity on the drying rate and drying constant of cocoa bean. Agricultural Engineering International: CIGR Journal, 2009.
[53]Taheri-Garavand, A., S. Rafiee, and A. Keyhani, Effect of temperature, relative humidity and air velocity on drying kinetics and drying rate of basil leaves. Electronic Journal of Environmental, Agricultural and Food Chemistry, 2011. 10(4): p. 2075-2080.
[54]Chamoli, S., P. Yu, and S. Yu, Multi-objective shape optimization of a heat exchanger tube fitted with compound inserts. Applied Thermal Engineering, 2017. 117: p. 708-724.